Journal of Materials Chemistry B

Accepted Manuscript

ROYAL SOCIETY OF CHEMISTRY

www.rsc.org/materialsB

Journal of Materials Chemistry B RSCPublishing

Paper

Electrospun Rubber Fibre Mats with Electrochemically Controllable Pore Sizes

Cite this: DOI: 10.1039/xoxxoooooox

Thomas E. Kerr-Phillips[a,b], Vincent Woehling[b,c], Remi Agniel[c], Giao T. M. Nguyen[c], Frederic Vidal[c], Paul Kilmartin[a], Cédric Plesse[c,]*, Jadranka Travas-Sejdic[a,]*

Received ooth January 2012,
Accepted ooth January 2012

DOI: 10.1039/xoxxoooooox

www.rsc.org/

ABSTRACT: Electroactive, elastomeric, microfiber mats that show controllable pore size variation upon electrochemical stimulation are produced from semi-interpenetrating polymer networks (s-IPNs). This type of porous, elastomeric scaffolds that are mechanically dynamic under electrochemical stimuli could find new applications in stretchable electronics, (bio)filtration, soft robotics and stimulation of biological cells. These microfiber mats are prepared in two simple steps. Firstly, a mixture of high molecular weight nitrile butadiene rubber (NBR) and cross-linking agent, poly(ethylene glycol)dimethylacrylate are electrospun with in situ cross-linking. Secondly, a conducting polymer poly(3,4-ethylenedioxythiophene) (PEDOT) is embedded into the electrospun fibres by oxidative chemical polymerization of EDOT-swollen microfiber mats. This two-step process affords robust, highly flexible and conductive s-IPN microfiber mats. The microfiber mat undergoes a controllable pore size variation upon applying an electrochemical stimuli in the form of a reduction-oxidation cycle to the mats in an electrolyte. The maximum average pore size variation, measured in situ using confocal microscopy, is 25%, achieved in 1 M lithium bis-trifluoromethanesulfonimide (LiTFSI) in propylene carbonate (PC) for a potential step between +0.6 V to –0.5 V (vs. Ag wire). These mats also show pore size variation in a biologically compatible solution, phosphate buffered saline.

Introduction

Electrospinning is a well-known technique[1] that has gained a renewed attention with the recent drive in nanotechnology. The process is compatible with large scale production and can create micro- to nano-scale fibres through an electrically charged jet of a polymer solution. Electrospun fibrous materials possess several attractive attributes such as a 3D fibrous structure, high porosity and large surface area. While they have been proposed for numerous applications such as desalination membranes[2], filters[3, 4], polarized light sources[5], sensors[4, 6], solar cells[7] and scaffolds for tissue engineering[8, 9], thus far they have mostly been used as passive structural materials since their post-electrospinning structure is fixed. However, there are a few examples were the post-electrospinning morphology is dynamic, such as nanofibre bundle actuators for artificial muscles[10] and piezoelectric actuating fibres[11].

The post-fabrication control of the structure and other material properties can meet the increasing demand for dynamic micro/nanoscale smart materials, especially in biotechnology, for cell clinics[12], pathogen classification[13], odour detection[14] and within micropumps and micromuscles for microfluidic devices[14, 15]. It may open new perspectives in numerous applications, i.e. turning (bio)filtration into tunable biofiltration, or mechanically static scaffolds for tissue engineering into electrochemomechanically active stimulating scaffolds. A sensible route to implement such functionality would be the use of electroactive polymers, the size and shape of which can be modified under electrical stimulation. Within this class of material, electrically conducting polymers (ECP) have received increased attention in recent literature[16-22], particularly those based on poly(3,4-ethylenedioxythiophene) (PEDOT)[16, 20, 22, 23] and polypyrrole (PPy)[16, 17, 19, 21, 24]. When ECPs are electrochemically oxidized or reduced, usually at low potentials, insertion/expulsion of counter-ions between an

electrolyte and the ECP takes place leading to controllable volume changes in the material. These materials combine interesting features, such as softness, lightness and biocompatibility, and show significant promise for applications such as artificial muscles[24-31], DNA sensing[31-33], and electrochromic effects[31, 34, 35]. However, ECP's are usually limited by poor mechanical stability, and as such they need to be modified through the use of appropriate dopants[36] or through composites[34, 37, 38] and additives[36]. One approach to enhance the properties of ECPs is to incorporate them into a cross-linked structure, forming a semi-interpenetrating polymer network (s-IPN). An ECP s-IPN design, directed towards actuator applications, requires specific features. These include having rubbery properties so as not to hinder the electrically driven volume change in the actuating element, and to be cross-linked to avoid flow and creep during actuation. There are several reports on cross-linked electrospun fibres, mainly non-elastomeric fibres that have been cross-linked post-electrospinning, such as in the case of poly(vinyl alcohol)[39] (T_g of 85 °C) electrospun fibre mates or biopolymers such as collagen[40] or gelatin[41]. The lack of reports on cross-linked rubber electrospun fibres in the literature is understandable given that rubbers have a glass transition temperature (T_g) below room temperature. This causes the electrospun fibres to coalesce before effective cross-linking takes place and the fibrous morphology is no longer preserved. In the few described cases, butadiene rubber (BR) was cross-linked in situ with UV radiation[42-44].

Here, we report electrospun microfiber mats with dynamic electrochemical stimuli-controllable pore sizes through intrinsic elastomeric and electroactive properties. The material, an s-IPN, is comprised of a cross-linked nitrile butadiene rubber (NBR), and an electrically conducting polymer (PEDOT). The elastomeric scaffold is prepared by in situ cross-linking during the electrospinning of the microfibers, and PEDOT is then incorporated via vapour phase swelling of the fibres with the monomer, EDOT, followed by its oxidative polymerisation. The resulting 3D electroactive microfibrous structures are robust, exhibits solvent stability and combine the mechanical properties of the electrospun fibres and the electromechanical properties of the conducting polymer. The change in the pore sizes was characterized though confocal microscopy with in situ electrochemical stimulation in an organic electrolyte as well as in biologically important phosphate buffered saline (PBS) solution.

Experimental

Chemicals. NBR with 44% acetonitrile (ACN) was kindly provided by Lanxess (Mw = 230 000 gmol-1, Per-bunan 4456F). Chloroform, methanol, benzoyl peroxide (BPO), poly(ethylene glycol) dimethacrylate (PEGDM, Mn=550 g.mol-1), 2,2-dimethoxy-2-phenylacetophenone (Irgacure 651), propylene carbonate and phosphate buffer saline solution were purchased from Sigma Aldrich. An-hydrous iron III chloride was purchased from Acros, 3,4-ethylenedioxythiophene (EDOT) (H C Starck) was dis-tilled under reduced pressure before use. Lithium bis-trifluoromethanesulfonimide (LiTFSI) from Solvay. All materials were used as received unless otherwise stated.

Electrospinning NBR/PEGDM. The electrospinning solutions (Table 1) were prepared by dissolving NBR in chloroform until homogenous solutions were obtained. This is followed by the addition of the corresponding amounts of poly(ethylene glycol)dimethacrylate PEGDM (which was run through a basic activated alumina column before use to remove the inhibitor MEHQ), Irgacure 651 and benzoyl peroxide (BPO). The solution was further stirred until it became homogeneous and drawn into a 1 ml or 5 ml all glass syringe with an 18G metallic needle. The electrospinning was then performed using a 14 kV electric field, with a 10 cm needle-collector distance and 1.0 ml/h pump rate. In situ ¬cross-linking was achieved with the photoinitiator, Irgacure 651 and using an 80000 µW/cm2 UV lamp purchased from South West Pacific (model SB100P/FA). Further cross-linking was achieved though thermal initiator, BPO in a vacuum oven at 80° C under reduced pressure.

PEDOT Incorporation into NBR/PEGDM microfibers. The electrospun mats were swollen with 3,4-ethylenedioxythiophene (EDOT) using vapour phase deposition for 2-6 h achieving a swelling ratio of 80 – 120%. EDOT was then oxidized via immersing the swollen electrospun mat in an aqueous solution of 1.5 M FeCl3 for various times at 40 ° C (Table 2), resulting in polymerisation of the EDOT and forming the PEDOT interpenetrated elastomeric microfibers.

SEM and EDX analysis. SEM on samples with and without PEDOT was conducted with a Philips XL30S FEG with a SiLi (Lithium drifted) with a Super Ultra Thin Window EDS detector and with a LEICA LEO S430i SEM. The samples prior to PEDOT incorporation were coated with a Quorum Q150RS sputter coater to give a double layer of platinum coating. Samples for EDX and cross-section SEM images were cryocut in liquid nitrogen before imaging.

Bulk IPN Synthesis and characterisation. Non-electrospun bulk film samples were prepared from a solution containing 40 %wt polymer and 60 %wt CHCl3. The polymer weight percentage was comprised of NBR and PEGDM at a 100:56 ratio respectively. The photoinitiator (Irgacure 651) was then added at 5%, 10% and 20% of the NBR mass for the different samples (See supplementary information). The samples were prepared by setting the resulting viscous solution between two glass slides, separated by a 250 µm Teflon seal, clamped together and passed under a high intensity UV light source (100 Wcm-2) for 200 sec or for 300 sec. Soxhlet extraction was then performed in chloroform for 3 days in order to obtain the extractable content. The remaining samples were used for characterisation by DMA analysis and ionic conductivities in 1 M LiClO4 PC solution, PBS solution, and in 1 M LiTFSI PC solution. Ionic conductivity of the non-electrospun samples was performed using a VSP potentiometer (Biologic) over a frequency range from 0.01 Hz to 1 MHz. A perturbation of 10 mV was applied to the cell consisted of the sample sandwiching between two stainless steel electrodes. The conductivity value was calculated from the bulk resistance in the complex impedance diagram. During the test, the temperature was controlled by means of programmable hot plate cells. The samples were swollen in the corresponding electrolyte solution overnight before performing impedance. The values were recorded 3 times and aver-aged to take into account solvent evaporation.

Elemental analysis of PEDOT embedded microfiber mats. Elemental analysis was carried out by microanalysis department of ICSN-CNRS. The tests were made 3 times per samples in order to obtain an average.

Electrochemical Characterisation of the PEDOT embedded Microfiber Mats. Cyclic Voltammetry was carried out using a VSP potentiometer (Biologic) at 50 mV/s for samples in 1 M LiTFSi PC solution and PBS solution. For the samples in PBS solution the rate was also recorded at 5, 10, 20, and 100 mV/s. The fibre mats were placed in a gold mesh that was then used as the working electrode. Platinized titanium wire and silver wire were used as counter and reference electrodes, respectively. Conductance measurements were carried out using a KEITHLEY 2000 multimeter with gold contacts.

Confocal Microscopy analysis of PEDOT embedded microfiber mats. Pore size variation was visualised in situ by immersing the film in 1 M LiTFSI - PC solution or a PBS solution and using a confocal microscope to map and monitor the changes. The confocal microscope used was an inversed ZEISS Axio Lab A1 microscope with an x63 oil Plan Apo lens. The sample was in contact with a gold mesh as the working electrode under the control of an Autolab PGSTAT101 potentiostat, and used in con-junction with a platinized titanium counter and a silver reference electrode. The gold mesh was separated from the counter electrode by a poly(vinylidene fluoride) PVDF membrane. During the experiment potential was stepped from -0.5 to +0.6 V. Image analysis for SEM images and confocal microscopy images was performed using the ImageJ software package.

Results and Discussion

Electrospinning of elastomeric microfibers. The electrospun elastomeric scaffold was fabricated from a solution of $CHCl_3$ containing linear high molecular weight NBR and poly(ethylene glycol) dimethacrylate (PEGDM). NBR provides the rubbery properties while the PEGDM acts as a cross-linked. PEGDM was also expected to facilitate the subsequent PEDOT interpenetration into the NBR network due to the compatibilizing effect of ethylene oxide groups present on both the PEO and the PEDOT repetitive units[45, 46].

The glass transition temperature of NBR is below room temperature (Tg = -10 °C) and PEGDM is in a liquid state at the room temperature. Therefore in order to prevent coalescence of the electrospun fibres, in situ cross-linking had to be performed during the electrospinning. The free radical, UV photoinitiator (Irgacure 651) was added into the electrospinning solutions to cross-link the polymers during the electrospinning process[47]. The solution viscosity is a major variable in determining the fibre morphology during electrospinning and contributes to the fibre thickness and fibre beading[48, 49]. The PEGDM used in this work had a Mn of 550 g mol-1. It is a liquid with low viscosity (6.5 mPas-1) at room temperature and thus did not contribute to the viscosity as much as the high molecular weight NBR. The NBR concentration in the electrospinning solution was explored first while keeping the PEDGM proportion at 56 %wt/wt vs NBR (Table 1). The PEGDM ratio was set at this value in order to increase and optimize the compatibility with the PEDOT by the ethylene oxide group. Large beading occurred at 5% wt/vol of NBR (Figure S1), whereas much more uniform fibres were seen at 10% wt/vol with fibre diameters ranging from 3 to 6 µm. It was therefore decided to continue further experiments with 10% wt/vol of NBR.

The influence of the cross-linking initiators (Irgacure 651 and BPO) concentration on the fibre morphology was then studied. While low concentrations of the UV initiator (5 and 10 %wt vs NBR) produced descent fibres (creating a porous mat useful for applications such as filtration) (Figure 1a and Figure 1b respectively), the mats produced from these compositions lost their fibrous morphology upon solvent-facilitated detachment of the mats from the collector, indicating that they were insufficiently cross-linked. At higher initiator concentrations (20 %wt photoinitiator vs NBR) the resulting fibre morphology was inconsistent, with sporadic domains of highly fused fibres and relatively non-fused fibres (Figure 1c). This was attributed to cross-linking occurring inside the electrospinning syringe, which varied the solution composition that formed the electrospinning jet with time (i.e. a decreasing polymer concentration with time due to cross-linked polymer becoming trapped within the syringe). A free radical initiator for thermally induced polymerisation, benzoyl peroxide (BPO), was therefore added to the electrospinning solution in order to induce further thermal cross-linking in addition to UV-initiated cross-linking. The thermal cross-linking of the UV-cross-linked electrospun mats was performed at 80 °C in a vacuum oven after the electrospinning. While no obvious improvement in morphology was observed with the addition of the thermal initiator when a low UV initiator concentration (5 %wt Irgacure 651, and 5 %wt BPO) was employed (Figure 1d), quite uniform fibres (Figure 1e) were produced with a moderate UV initiator concentration (10 %wt Irgacure 651 and 5 %wt BPO). Increasing the concentration of both initiators further (20 %wt. Irgacure 651, 10 %wt. BPO) produced well-defined fibres, as depicted in Figure 1f. However significant cross-linking occurred in the syringe, which caused the syringe to jam, this lead to difficulty in producing free standing fibre mats.

The efficiency of the crosslinking was qualitatively determined by comparing SEM images before and after immersing of the samples in chloroform for three days - a good solvent for both NBR and PEGDM (**Figure 1**). The electrospun mats prepared with 10 %wt and 5 %wt of Irgacure 651 and BPO (vs NBR), respectively, presented the same fibrous morphology prior and post-soxhlet extraction in chloroform. The non-fusion of fibres in solvent can be considered as a strong evidence of efficient crosslinking of the material.

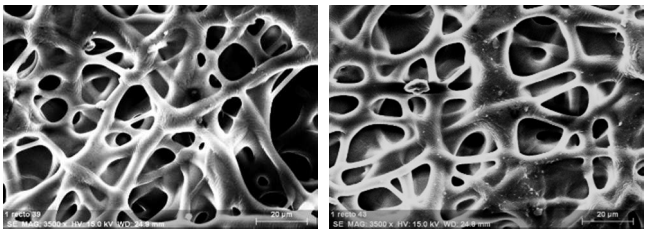

Figure 1 Microfiber electrospun mats before (left) and after (right) leaving in chloroform for 3 days; magnification × 3500. Samples prepared with 10 %wt and 5 %wt (vs NBR) of Irgacure and BPO, respectively.

To further investigate the efficiency of the crosslinking, non-electrospun bulk films of the same composition were prepared under similar conditions as the electrospun fibre mats. These films were UV cross-linked with a range of Irgacure 651 content, followed by the thermal crosslinking with BPO in some cases. All films were underwent a soxhlet extraction to determine the materials' extractable content. The films with 10

%wt and 5 %wt of the UV and the thermal initiators, respectively, showed effective crosslinking, with an extractible content of only approximately 4%. Ionic conductivity of the bulk films swollen in various electrolytes has been measured (See SI **Table S1)**, as an estimate of the ionic conductivity of the electrospun fibres of the same compositions. Values of 2 x 10^{-3} S.cm^{-1} ($LiClO_4$ 1M /PC), 1 x 10^{-3} S.cm^{-1} (LiTFSI 1M / PC), and 5 x 10^{-7} S.cm^{-1} (PBS) were measured for the films cross-linked with 10 %wt and 5 %wt of Irgacure and BPO (vs NBR). Since the ECP is subsequently interpenetrated within the host NBR fibres, these relatively high ionic conductivity values in organic electrolyte indicate that the ions should be mobile enough to facilitate good actuation of the incorporated PEDOT. However, the low value in PBS should lead to a lower actuation, since the electroactive polymer that will be subsequently interpenetrated in the mats will be poorly accessible for ions from the PBS solution.

Table 1. Compositions of the electrospinning chloroform solutions. Average fibre diameter and average pore area were determined from SEM images (n = 10)

Sample No.	NBR (%wt/vol)	PEGDMA (%wt/wt NBR)	Irgacure 651 (%wt/wt NBR)	Benzoyl Peroxide (%[a])	Average Fibre Diameter (µm)	Average Pore Area (µm)
A	10	56	5	0	3.6 ± 1.3	87± 46
B	10	56	10	0	5.3 ± 2.1	141 ± 85
C	10	56	20	0	4.2 ± 1.6	136 ± 68
D	10	56	5	5	6.2 ± 2.3	118 ±92
E	10	56	10	5	2.5 ± 1.6	52 ± 35
F	10	56	20	10	6.0 ± 1.8	N/A
G	10	150	20	0	N/A	N/A
H	10	150	20	10	14.7 ± 8.4	N/A

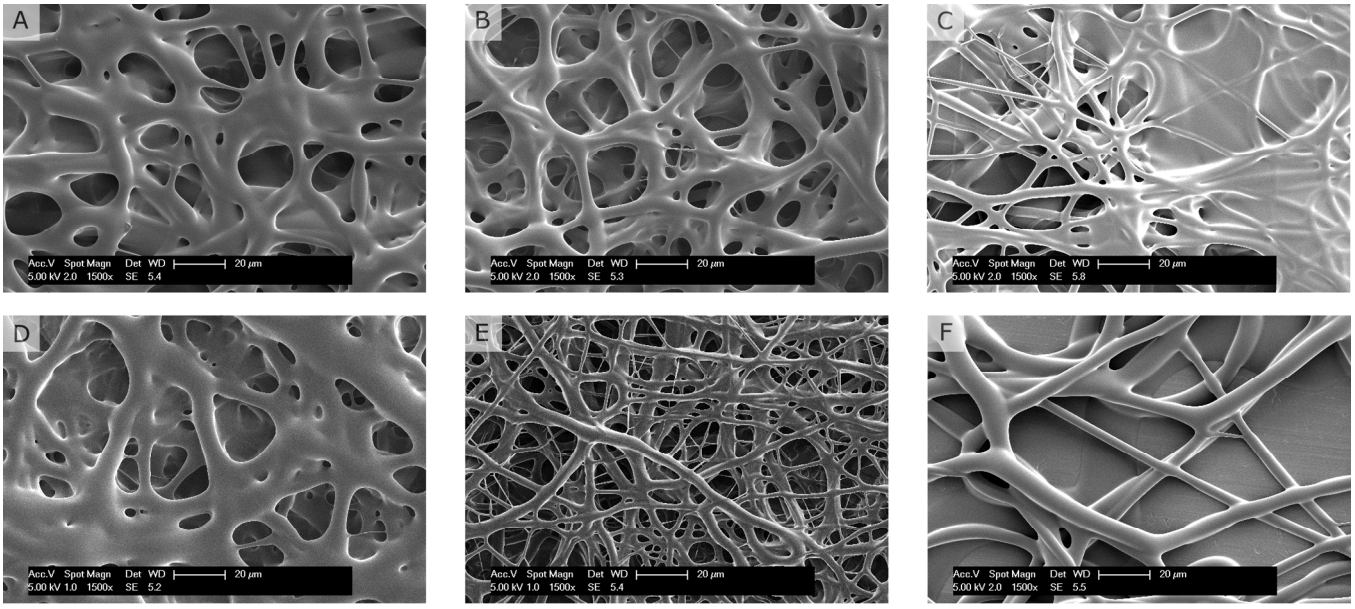

Figure 2 Electrospun NBR/PEGMA elastomeric fibres: electrospun from 10 %wt. NBR solution in chloroform with various % (vs. NBR) of the photoinitiator Irgacure 651; NBR:PEGDM ratio (wt/wt) of 100:56; magnification x 1500 (bar = 20 µm). Images A-F refer to samples A to F in Table 1, respectively.

Journal of Materials Chemistry B RSCPublishing

Paper

In summary, a solution composition of 10 %wt/vol of NBR, 56 %wt (vs NBR) of PEGDM, 10 %wt (vs NBR) of Irgacure 651 and 5 %wt (vs NBR) of BPO was determined to provide fibre mats with the best fibre morphology (Sample 5, Table 1 and Figure 2e) out of the investigated compositions, as it afforded uniform cross-linked fibres with the least coalescence. Thus, subsequent experiments were undertaken on this particular fibre mat composition.

Preparation of the electroactive, elastomeric microfiber mats. Interpenetration of PEDOT into a host polymer matrix can be achieved through swelling of the host matrix with EDOT monomer in liquid or gas phase followed by immersion in oxidative solution (such as aqueous ferric chloride) to induce oxidative chemical polymerization[50, 51]. The use of an aqueous oxidant solution plays an important role here due to the low miscibility of EDOT in water. This prevents excessive leaching

Journal of Materials Chemistry B RSCPublishing

Paper

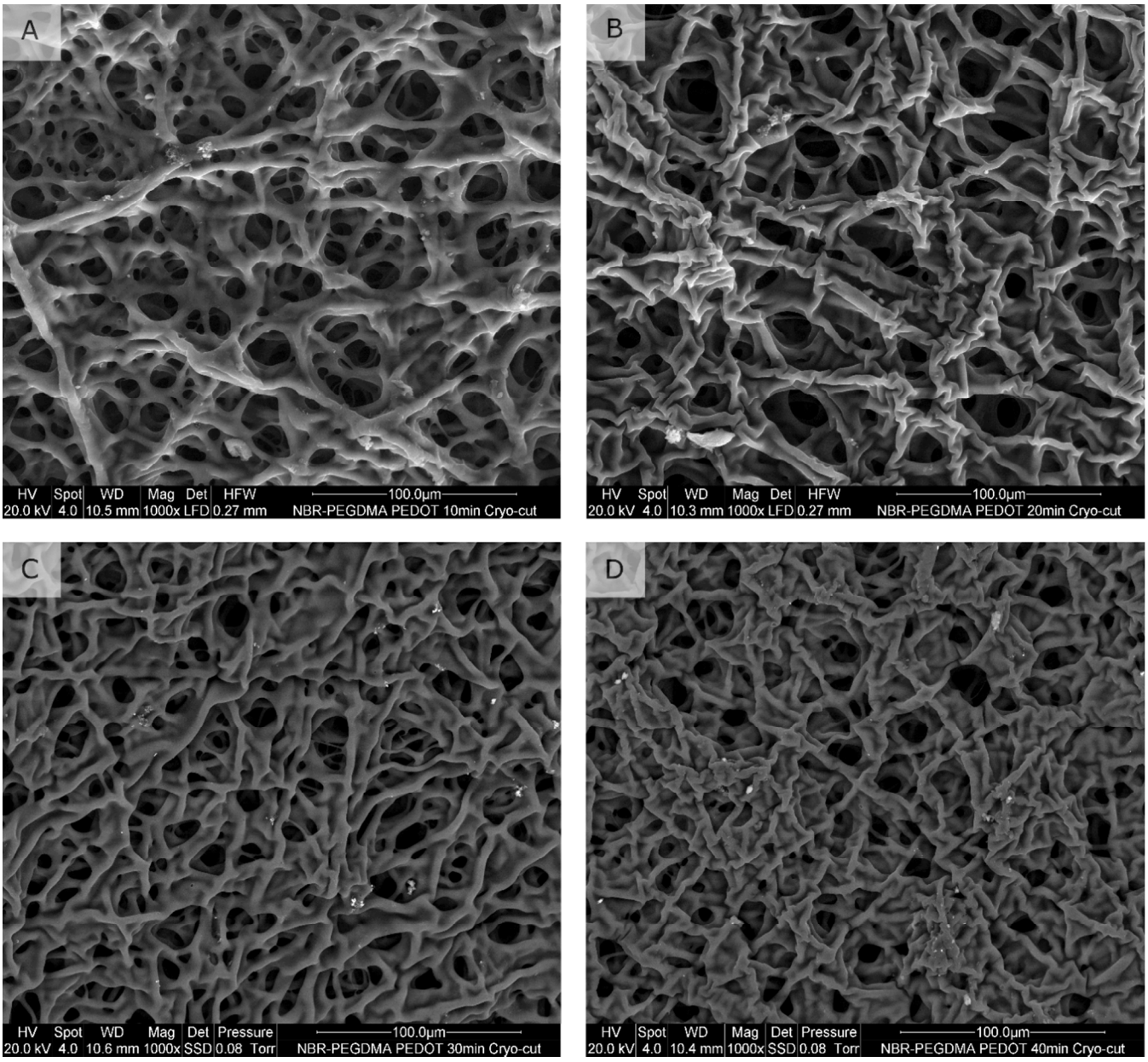

Figure 3 S-IPN NBR/PEGDMA/PEDOT fibre mats with PEDOT polymerization times of: A. 10 min, B. 20 min, C. 30 min and D. 40 min.

of EDOT in water. This prevents excessive leaching of EDOT from the host matrix into the solution during EDOT polymerisation. The procedure leads to a gradient distribution of PEDOT in the host polymer, i.e. high content of PEDOT near the surface and lower near the centre. As this approach has proven to be successful previously[50], it was adapted in this work. EDOT was incorporated into the electrospun mats by gas phase swelling under reduced pressure of 10-2 mbar until a swelling ratio of 120% was reached[50]. The EDOT-swollen fibre mats were then immersed in 1.5 M $FeCl_3$ (aq.) to polymerize EDOT. Polymerization times between 10 and 60 min were explored. As determined by elemental analysis the PEDOT content in the s-IPN fibre mats increased linearly from 5 to 20 %wt for polymerization times between 10 to 40 min. At the

same time the electrical resistance decreased from 400 to 25 Ohms, as expected, indicating high surface electronic conductivity for high PEDOT content **(Figure 5)**.

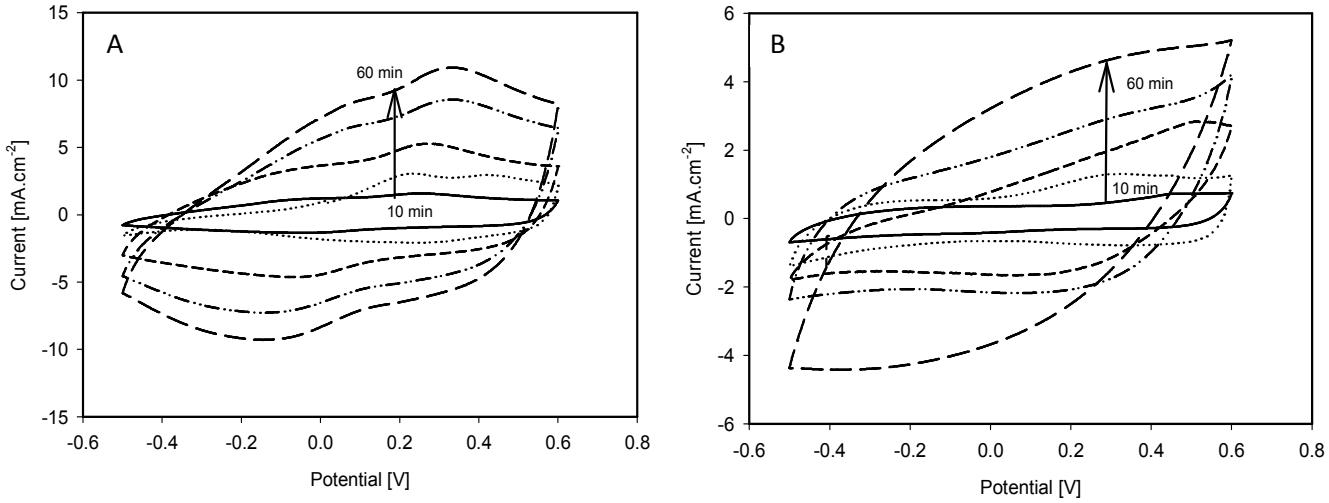

Figure 4 Cyclic voltamogramms of PEDOT embedded electrospun mats in a) 1 M LiTFSI PC solution and b) PBS solution. The arrow indicate increasing PEDOT polymerisation time of 10, 20, 30, 40 and 60 min.

The pore morphology of the s-IPN fibre mats was modified by the presence of PEDOT; the higher the content of PEDOT the lower the porosity of the fibre mats, as revealed by SEM images (**Figure 3)**. The EDOT swelling time and the polymerisation time therefore provides a way to fine tune the fibre mat porosity. Here, to balance the conductance and the average porosity of the mats the polymerisation time of 20 min (Figure 3B) was chosen for the actuation experiments (later in the Section 2.3).

EDX analysis was performed on the cross-sections of the fibre mats to determine the PEDOT distribution within the fibres. As observed in **Figure 6 (**and **Figures S2** to **S6)**, the sulphur atom, which is a chemical signature of the PEDOT repeat units, was mainly present near the surface of the fibres and not in their centres[50].

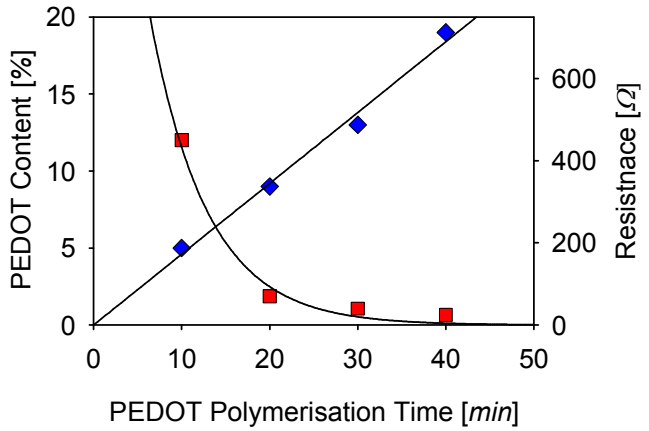

Figure 5 PEDOT content (♦) (R^2 = 0.994) and surface resistance (■) versus PEDOT polymerization time of conducting fibre mats.

The electroactivity of the fibre mats was characterized by cyclic voltammetry (CV). The CV experiments were performed in two electrolyte solutions, aqueous PBS, and 1 M LiTFSI in PC, and the recorded currents were normalised against the surface area of the fibre mats (**Figure 4**). With increasing PEDOT content, the fibre mats presented an increase in redox current corresponding to a higher electroactivity (note: the mats for these experiments were from the same piece of the electrospun fibre mat to avoid variation in the fibre mat morphology). The anodic and cathodic peak positions are in agreement with literature values for PEDOT[52-54]. The gradual shift to more anodic currents as polymerization time increases is attributed to the increased PEDOT content, causing a thicker, denser PEDOT layer on the fibre shell thus limiting ion diffusion.

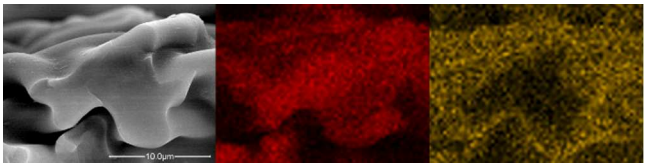

Figure 6 SEM image (left) and SEM EDX images showing elemental mapping for carbon (centre) and sulphur (right); magnification × 8000.

While excellent electroactivity was seen in propylene carbonate, a more resistive behaviour was observed in the PBS, as predicted from ionic conductivity measurements. These results are consistent with behaviour typically seen with PEDOT embedded IPN architecture. Indeed NBR and hydrophilic PEGDM chains can be swollen by PC allowing ion diffusion into and out of the interpenetrated PEDOT layer, which increases the electroactivity of the conducting layer; the ionic conductivity values of the non-electrospun films support this hypothesis. On the other hand, it is well known that pure PEDOT, due to hydrophobic domains and its conjugated

structure, does not swell well in water[55]. Moreover PEDOT chains are here interpenetrated within hydrophobic NBR chains. As a consequence the interpenetrated electrodes remain much less accessible to the ions of the PBS solution. However, the presence of hydrophilic PEGDM in the electrospun fibres may contribute to the observed (although lower) electroactivity in PBS, in a similar way to the effect seen in PEDOT grafted with polymeric hydrophilic grafts[56, 57].

In conclusion, embedding the elastomeric, electrospun mats through the EDOT vapour phase swelling method produced electroactive electrospun fibres with a decreasing gradient of PEDOT towards the centre of the fibres. These fibres then showed electroactivity in organic and aqueous electrolytes. The electroactivity of the fibre mats in PBS aqueous solution indicates the applicability of such materials in applications of biological relevance.

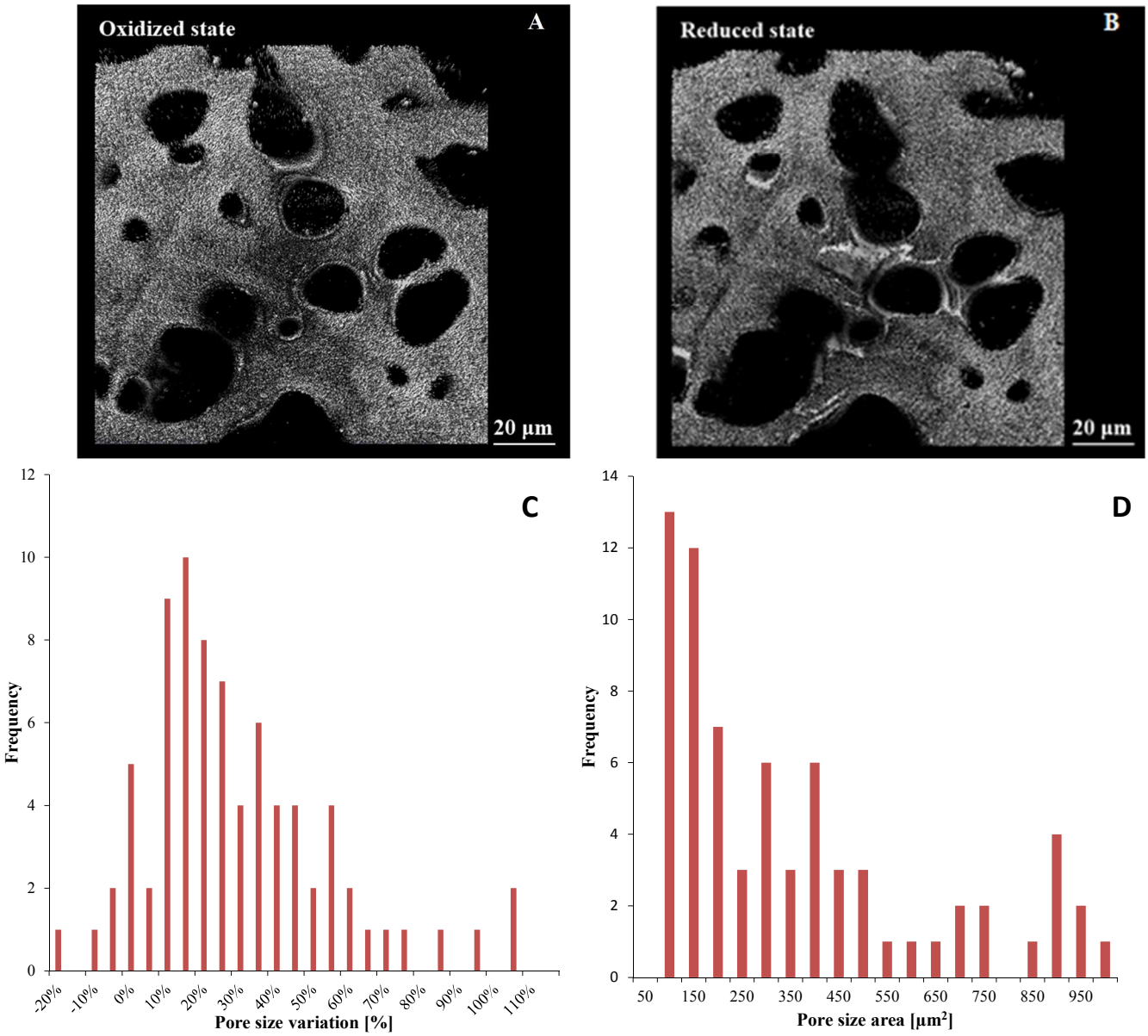

Figure 7 Topography mode confocal microscope images of the fibrous mat (9% PEDOT, 20 min polymerized) in 1 M LiTFSI PC, in oxidised state (A) and in reduced state (B) of a 3 µm slice. Pore size area distribution graphs (C) and pore size variation from oxidized to reduced state (D) obtained from the analysis of 80 pores.

Electrochemomechanical Actuation and Control of the Pore Sizes. The PEDOT (9 %wt, corresponding 20 min of polymerization) s-IPN fibre mat samples (1 × 1 cm) were stimulated under square wave potential at a frequency of 6.66×10^{-2} Hz. The potential window was chosen on the basis of the CVs of the material, in 1 M LiTFSI PC and PBS electrolytes (oxidation at + 0.6 V and reduction at – 0.5 V), in order to avoid over-oxidation or over-reduction and degradation of the material. Visualization of the change in the pore sizes upon actuation was achieved through confocal microscopy while the fibre mats were electrochemically stimulated in situ in an electrochemical cell (**Figure 8A**). Detailed confocal

microscopy images showing slices of 3 µm thick samples were obtained in reflectance mode (**Figure 8B** and **Figure 8C**) and in topography mode (**Figure 7A** and **Figure 7B**). The video recording of the pore size variation was made with the microscope in reflectance mode (**Figure S10**).

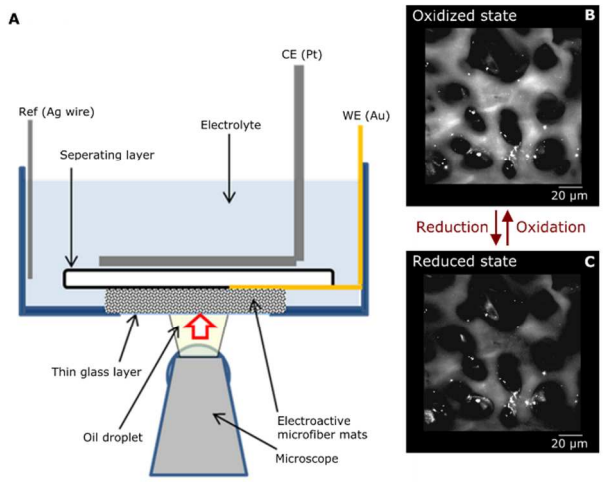

Figure 8 Confocal microscope measurement setup (A), reflectance mode confocal microscopy images of the fibrous mats in 1 M LiTFSI PC, for the oxidized (B) and the reduced (C) fibre mat.

Figure 7A and Figure 7B shows topography mode confocal microscopy images over a depth of 3 µm of the fibre mat in the oxidized and reduced state respectively in 1 M LiTFSI in PC. On the confocal microscope images, black areas represent the pore cavities while the bright areas correspond to the fibres. The area of the bright domains is increasing during the oxidation process corresponding to a volume increase of the ECP. This result indicates that the large solvated $TFSi^-$ anions are drawn into the oxidized PEDOT as counter-ions, causing fibre swelling and hence lowering the volume of the pores. This anion driven mechanism is consistent with the actuation of PEDOT in LiTFSi PC electrolyte[58, 59]. Conversely, in the reduced state, the solvated ion expulsion generates a fibre contraction in all directions, thus resulting in pore opening. The pore size and pore size variation were then calculated from the topography images (Figure 7A, 7B) on a total of 80 pores. An average area of 450 μm^2 and average pore diameter of 24 µm were determined for the oxidized state (**Figure 7C**). After reduction a large distribution of pore size variation was observed with an average increase in the pore sizes of 25% (**Figure 7D**).

The pore size change kinetics has been analysed over two redox cycles in the reflectance mode. Total pore size areas and the corresponding total pore size changes were calculated by image analysis and shown in **Figure 9**. Even at the low potential applied [-0.5 V / +0.6 V] a relatively fast response was observed with a maximum pore size change obtained after 15 s for oxidation and reduction processes and with a maximum strain speed of 4 % s^{-1}. A full recovery of the average pore size variation was obtained over the two cycles.

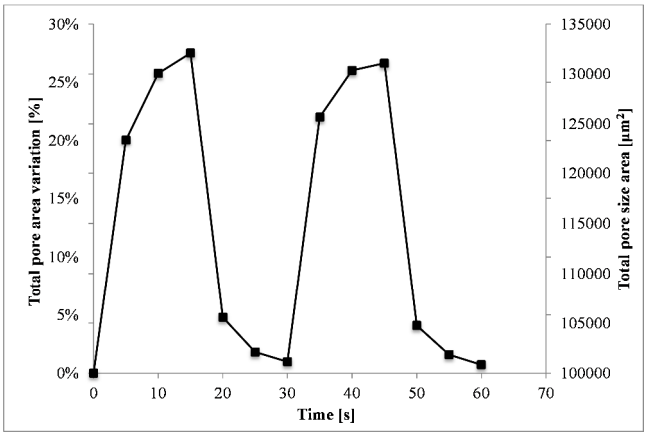

Figure 9 Variation of the pore size changes (left axes) and total pore size area (right axes) over time upon 2 oxidation/reduction cycles; the total sample area was 10000 μm^2.

The electromechanical behaviour of the mats was also studied in phosphate buffer saline (PBS) since this solution is commonly used in biological and medical research. Pore size changes in PBS under electrical stimulation was confirmed in both reflective and topography mode (**Figure S7** and **Figure S8**). Measurements were performed on 45 pores with an average diameter of 22.5 µm (400 μm^2 of the total pore area). Similar to actuation in 1 M LiTFSI in PC the pore sizes increased during the reduction of PEDOT, indicating that the Cl^- anion in the PBS solution is mainly responsible of the mechanical response. The mean pore size variation reached 4.7%, with a narrower distribution than in LiTFSI-PC electrolyte (**Figure S9**). The amplitude of the electromechanical response in PBS was smaller than in the LiTFSI/PC electrolyte, as expected based on the lower electroactivity of the fibre mats observed in CVs, the low ionic conductivity of the NBR/PEGDM material in PBS, and the size of solvated Cl- (0.332 nm)[60] ion compared to solvated TFSI- (ionic radii of 0.439 nm[61], solvation radii in acetonitrile of 2.24 nm[62]). These results demonstrate that electrochemomechanical response of the electroactive fibre mats is possible in biologically compatible solutions and opens up promising perspectives in biotechnological applications, for example, tissue engineering scaffolds.

Conclusions

For the first time the fabrication of novel, electroactive, elastomeric, non-woven, electrospun microfiber mats that undergo a reversible change in pore sizes was reported, resulting in a robust fabric with a controllable micron scale porosity. The fibres are comprised of cross-linked NBR/PEGDM and are made electroactive by the interpenetration of conducting polymer PEDOT. Synthesis of the microfiber mat was optimized and led to 3D fibrous scaffold with an average pore size of 25 ± 10 µm. After PEDOT incorporation, these conducting mats showed excellent electroactivity and reversible pore size variation and control upon electrical stimulation in an electrolyte solution. A maximum pore size variance of 25% has been observed in 1 M LiTFSI in PC and 5% in PBS. These mats are ideal candidates

for applications such as tunable filters of substances in the micron range, such as biological entities, or as 3D- scaffolds for mechanical-transduction studies of cells.

Acknowledgements

Mr. T. E. Kerr-Phillips acknowledges the MacDiarmid Institute for Advanced Materials and Nanotechnology, New Zealand for the PhD scholarship. Mr. V. Woehling thanks the Campus France agency for the funding.

Notes and references

[a] Polymer Electronics Research Centre (PERC), School of Chemical Sciences, University of Auckland, 23 Symonds Street, Auckland, New Zealand.

[b] These authors contributed equally.

[c] LPPI-EA2528, Institut des Materiaux, 5 mail Gay Lussac, Neuville sur Oise, Cergy-Pontoise cedex 95031, France.

* Corresponding Authors E-mail: j.travas-sejdic@auckland.ac.nz, E-mail: cedric.plesse@u-cergy.fr

Electronic Supplementary Information (ESI) available: Video showing pore size variation in 1 M LiTFSI PC solution, properties and compositions of non-electrospun films, SEM and EDX of electrospun microfibers and PEDOT embedded fibres respectively, and confocal microscopy and pore size variation data for microfiber mats in PBS solution. See DOI: 10.1039/b000000x/

1. J. Doshi and D. H. Reneker, *Journal of Electrostatics*, 1995, **35**, 151-160.
2. C.-I. Su, J.-H. Shih, M.-S. Huang, C.-M. Wang, W.-C. Shih and Y.-s. Liu, *Fibers Polym*, 2012, **13**, 698-702.
3. Y. Guibo, Z. Qing, Z. Yahong, Y. Yin and Y. Yumin, *Journal of Applied Polymer Science*, 2013, **128**, 1061-1069.
4. R. Sahay, P. S. Kumar, R. Sridhar, J. Sundaramurthy, J. Venugopal, S. G. Mhaisalkar and S. Ramakrishna, *Journal of Materials Chemistry*, 2012, **22**, 12953-12971.
5. K. Yin, L. Zhang, C. Lai, L. Zhong, S. Smith, H. Fong and Z. Zhu, *Journal of Materials Chemistry*, 2011, **21**, 444-448.
6. D. Aussawasathien, J. H. Dong and L. Dai, *Synthetic Metals*, 2005, **154**, 37-40.
7. C. Drew, X. Wang, K. Senecal, H. Schreuder-Gibson, J. He, J. Kumar and L. A. Samuelson, *Journal of Macromolecular Science, Part A*, 2002, **39**, 1085-1094.
8. M. Gizdavic-Nikolaidis, S. Ray, J. R. Bennett, A. J. Easteal and R. P. Cooney, *Macromolecular Bioscience*, 2010, **10**, 1424-1431.
9. W.-J. Li, C. T. Laurencin, E. J. Caterson, R. S. Tuan and F. K. Ko, *Journal of Biomedical Materials Research*, 2002, **60**, 613-621.
10. B. K. Gu, Y. A. Ismail, G. M. Spinks, S. I. Kim, I. So and S. J. Kim, *Chemistry of Materials*, 2009, **21**, 511-515.
11. J. Pu, X. Yan, Y. Jiang, C. Chang and L. Lin, *Sensors and Actuators A: Physical*, 2010, **164**, 131-136.
12. E. H. Jager, C. Immerstrand, K. Peterson, K.-E. Magnusson, I. Lundström and O. Inganäs, *Biomedical Microdevices*, 2002, **4**, 177-187.
13. E. Smela, M. Christophersen, S. B. Prakash, M. Urdaneta, M. Dandin and P. Abshire, 2007, pp. 65240G-65240G-65210.
14. T. F. Otero, J. G. Martinez and J. Arias-Pardilla, *Electrochimica Acta*, 2012, **84**, 112-128.
15. C. Immerstrand, K. Holmgren-Peterson, K.-E. Magnusson, E. Jager, M. Krogh, M. Skoglund, A. Selbing and O. Inganäs, *MRS Bulletin*, 2002, **27**, 461-464.
16. U. L. Zainudeen, M. A. Careem and S. Skaarup, *Sensors and Actuators B: Chemical*, 2008, **134**, 467-470.
17. F. Vidal, C. Plesse, G. Palaprat, A. Kheddar, J. Citerin, D. Teyssié and C. Chevrot, *Synthetic Metals*, 2006, **156**, 1299-1304.
18. S. Radhakrishnan and S. B. Kar, *Sensors and Actuators B: Chemical*, 2006, **119**, 94-98.
19. R. Kiefer, R. Temmer, T. Tamm, J. Travas-Sejdic, P. A. Kilmartin and A. Aabloo, *Synthetic Metals*, 2013, **171**, 69-75.
20. J. Ding, L. Liu, G. M. Spinks, D. Zhou, G. G. Wallace and J. Gillespie, *Synthetic Metals*, 2003, **138**, 391-398.
21. R. Kiefer, S. Y. Chu, P. A. Kilmartin, G. A. Bowmaker, R. P. Cooney and J. Travas-Sejdic, *Electrochimica Acta*, 2007, **52**, 2386-2391.
22. R. Kiefer, G. A. Bowmaker, R. P. Cooney, P. A. Kilmartin and J. Travas-Sejdic, *Electrochimica Acta*, 2008, **53**, 2593-2599.
23. M. Fuchiwaki, K. Tanaka and K. Kaneto, *Sensors and Actuators A: Physical*, 2009, **150**, 272-276.
24. I. S. Romero, N. P. Bradshaw, J. D. Larson, S. Y. Severt, S. J. Roberts, M. L. Schiller, J. M. Leger and A. R. Murphy, *Advanced Functional Materials*, 2014, **24**, 3866-3873.
25. R. Kiefer, G. A. Bowmaker, P. A. Kilmartin and J. Travas-Sejdic, *Electrochimica Acta*, 2010, **55**, 681-688.
26. R. Kiefer, D. G. Weis, J. Travas-Sejdic, G. Urban and J. Heinze, *Sensors and Actuators B: Chemical*, 2007, **123**, 379-383.
27. R. H. Baughman, *Synthetic Metals*, 1996, **78**, 339-353.
28. C. Plesse, F. Vidal, D. Teyssie and C. Chevrot, *Chemical Communications*, 2010, **46**, 2910-2912.
29. C. Laslau, D. E. Williams, B. E. Wright and J. Travas-Sejdic, *Journal of the American Chemical Society*, 2011, **133**, 5748-5751.
30. R. Kiefer, X. Mandviwalla, R. Archer, S. S. Tjahyono, H. Wang, B. MacDonald, G. A. Bowmaker, P. A. Kilmartin and J. Travas-Sejdic, 2008, pp. 69271E-69271E-69211.
31. T. F. Otero and J. G. Martinez, *Journal of Materials Chemistry B*, 2013, **1**, 26-38.
32. H. Peng, L. Zhang, C. Soeller and J. Travas-Sejdic, *Biomaterials*, 2009, **30**, 2132-2148.
33. J. Travas-Sejdic, N. Aydemir, B. Kannan, D. E. Williams and J. Malmstrom, *Journal of Materials Chemistry B*, 2014, **2**, 4593-4609.
34. D. Mecerreyes, R. Marcilla, E. Ochoteco, H. Grande, J. A. Pomposo, R. Vergaz and J. M. Sánchez Pena, *Electrochimica Acta*, 2004, **49**, 3555-3559.
35. P. Verge, P.-H. Aubert, F. Vidal, L. Sauques, F. Tran-Van, S. Peralta, D. Teyssié and C. Chevrot, *Chemistry of Materials*, 2010, **22**, 4539-4547.
36. L. Yuechen, T. Ryo and O. Hidenori, *Smart Materials and Structures*, 2014, **23**, 074010.
37. G. Latessa, F. Brunetti, A. Reale, G. Saggio and A. Di Carlo, *Sensors and Actuators B: Chemical*, 2009, **139**, 304-309.
38. X. Sui, X. Feng, M. A. Hempenius and G. J. Vancso, *Journal of Materials Chemistry B*, 2013, **1**, 1658-1672.
39. S. Agarwal, A. Greiner and J. H. Wendorff, *Advanced Functional Materials*, 2009, **19**, 2863-2879.
40. M. Angarano, S. Schulz, M. Fabritius, R. Vogt, T. Steinberg, P. Tomakidi, C. Friedrich and R. Mülhaupt, *Advanced Functional Materials*, 2013, **23**, 3277-3285.
41. Y. Z. Zhang, J. Venugopal, Z. M. Huang, C. T. Lim and S. Ramakrishna, *Polymer*, 2006, **47**, 2911-2917.
42. S. S. Choi, J. P. Hong, Y. S. Seo, S. M. Chung and C. Nah, *Journal of Applied Polymer Science*, 2006, **101**, 2333-2337.
43. M. Tian, Q. Hu, H. Wu, L. Zhang, H. Fong and L. Zhang, *Materials Letters*, 2011, **65**, 3076-3079.
44. Q. Hu, H. Wu, L. Zhang, H. Fong and M. Tian, *Express Polymer Letters*, 2012, **6**, 258-265.
45. F. Vidal, C. Plesse, P.-H. Aubert, L. Beouch, F. Tran-Van, G. Palaprat, P. Verge, P. Yammine, J. Citerin, A. Kheddar, L. Sauques, C. Chevrot and D. Teyssié, *Polymer International*, 2010, **59**, 313-320.
46. F. Vidal, J. F. Popp, C. Plesse, C. Chevrot and D. Teyssié, *Journal of Applied Polymer Science*, 2003, **90**, 3569-3577.
47. S. Kalakkunnath, D. S. Kalika, H. Lin and B. D. Freeman, *Journal of Polymer Science Part B: Polymer Physics*, 2006, **44**, 2058-2070.
48. H. Fong, I. Chun and D. H. Reneker, *Polymer*, 1999, **40**, 4585-4592.

49. J. H. Yu, S. V. Fridrikh and G. C. Rutledge, *Polymer*, 2006, **47**, 4789-4797.
50. A. Maziz, C. Plesse, C. Soyer, C. Chevrot, D. Teyssié, E. Cattan and F. Vidal, *Advanced Functional Materials*, 2014, **24**, 4851-4859.
51. N. Festin, A. Maziz, C. Plesse, D. Teyssié, C. Chevrot and F. Vidal, *Smart Materials and Structures*, 2013, **22**, 104005.
52. V. Noël, H. Randriamahazaka and C. Chevrot, *Journal of Electroanalytical Chemistry*, 2003, **542**, 33-38.
53. H. Randriamahazaka, C. Plesse, D. Teyssié and C. Chevrot, *Electrochemistry Communications*, 2003, **5**, 613-617.
54. L. J. del Valle, D. Aradilla, R. Oliver, F. Sepulcre, A. Gamez, E. Armelin, C. Alemán and F. Estrany, *European Polymer Journal*, 2007, **43**, 2342-2349.
55. S. S. Kumar, J. Mathiyarasu and K. L. Phani, *Journal of Electroanalytical Chemistry*, 2005, **578**, 95-103.
56. L. Strover, C. Roux, J. Malmström, Y. Pei, D. E. Williams and J. Travas-Sejdic, *Synthetic Metals*, 2012, **162**, 381-390.
57. J. Malmström, M. K. Nieuwoudt, L. T. Strover, A. Hackett, O. Laita, M. A. Brimble, D. E. Williams and J. Travas-Sejdic, *Macromolecules*, 2013, **46**, 4955-4965.
58. F. Carpi, R. Kornbluh, P. Sommer-Larsen and G. Alici, *Bioinspiration & Biomimetics*, 2011, **6**, 045006.
59. T. Rauno, A. Maziz, C. Plesse, A. Aabloo, F. Vidal and T. Tamm, *Smart Materials and Structures*, 2013, **22**, 104006.
60. E. R. Nightingale, *The Journal of Physical Chemistry*, 1959, **63**, 1381-1387.
61. S. Zhang, N. Sun, X. He, X. Lu and X. Zhang, *Journal of Physical and Chemical Reference Data*, 2006, **35**, 1475-1517.
62. R. Lin, P. Huang, J. Ségalini, C. Largeot, P. L. Taberna, J. Chmiola, Y. Gogotsi and P. Simon, *Electrochimica Acta*, 2009, **54**, 7025-7032.

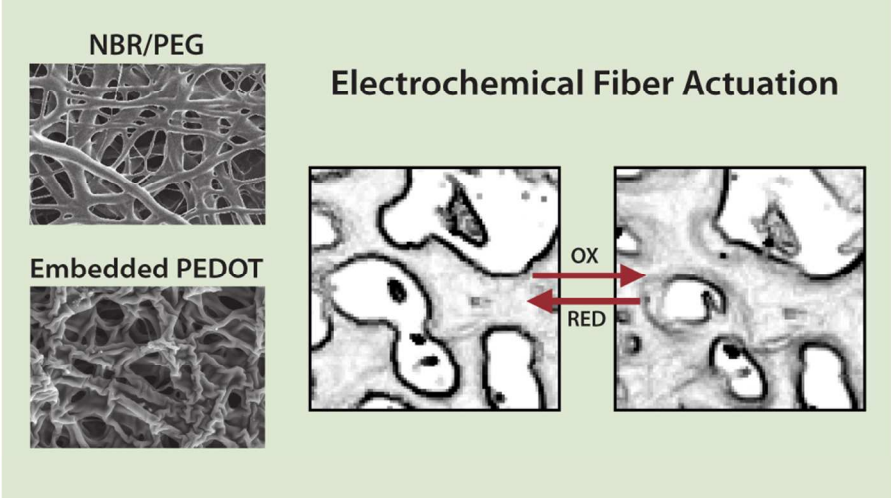

95x52mm (300 x 300 DPI)